# Converging evidence for functional and structural segregation within the left ventral occipitotemporal cortex in reading

Garikoitz Lerma-Usabiaga[a,b,1], Manuel Carreiras[a,c,d], and Pedro M. Paz-Alonso[a]

[a]BCBL, Basque Center on Cognition, Brain and Language, San Sebastián, 20009 Gipuzkoa, Spain; [b]Department of Psychology, Stanford University, Stanford, CA 94305; [c]IKERBASQUE, Basque Foundation for Science, 48013 Bilbao, Bizkaia, Spain; and [d]Departamento de Lengua Vasca y Comunicación, Euskal Herriko Unibertsitatea/Universidad del País Vasco, 48940 Leioa, Bizkaia, Spain

Edited by Michael I. Posner, University of Oregon, Eugene, OR, and approved August 14, 2018 (received for review February 21, 2018)

**The ventral occipitotemporal cortex (vOTC) is crucial for recognizing visual patterns, and previous evidence suggests that there may be different subregions within the vOTC involved in the rapid identification of word forms. Here, we characterize vOTC reading circuitry using a multimodal approach combining functional, structural, and quantitative MRI and behavioral data. Two main word-responsive vOTC areas emerged: a posterior area involved in visual feature extraction, structurally connected to the intraparietal sulcus via the vertical occipital fasciculus; and an anterior area involved in integrating information with other regions of the language network, structurally connected to the angular gyrus via the posterior arcuate fasciculus. Furthermore, functional activation in these vOTC regions predicted reading behavior outside of the scanner. Differences in the microarchitectonic properties of gray-matter cells in these segregated areas were also observed, in line with earlier cytoarchitectonic evidence. These findings advance our understanding of the vOTC circuitry by linking functional responses to anatomical structure, revealing the pathways of distinct reading-related processes.**

visual word recognition | visual word form area | functional and structural MRI | reading | quantitative MRI

Over 15 y ago, Cohen, Dehaene, and coworkers described a standard reading model (1, 2). In this model, they named a word-responsive patch within the ventral occipitotemporal cortex (vOTC) the "visual word form area" (VWFA) and proposed that this region was involved in identifying word forms. Nevertheless, due to heterogeneous experimental procedures and the intrinsic limitations of functional and structural MRI tools, the specific cortical localization of the VWFA typically differs between studies, and it has been proposed that there may be more than one VWFA (e.g., refs. 3–7). It is further expected that adjacent VWFA tissue performs distinct computations and that these different regions may be in charge of different functions related to the visual word-recognition process. The present study combines functional localizers, structural (diffusion-weighted), and cytoarchitectonic-related MRI data [i.e., T1 relaxation times; macromolecular tissue volume (MTV)] with behavioral data in the same individual space to characterize the vOTC circuitry involved in visual word recognition.

Previously, separate functional (4, 7), structural (5, 8–10), and cytoarchitechtonic (11–13) evidence has highlighted the possibility that different regions within or adjacent to the occipitotemporal sulcus (OTS) are involved in distinct processes of visual word recognition. Functionally, word identification entails processing three main components: (*i*) the general visual information composed of light and dark patches, (*ii*) the word as a uniquely shaped visual unit (the word form), and (*iii*) the word as a language unit. We hypothesize that this processing takes place in distinct vOTC regions that can be identified by means of functional contrasts widely used in previous research and that can be organized into two groups: (*i*) contrasts that isolate the word as a language unit signal, and (*ii*) contrasts that isolate the word as a language unit and the visual word form signal, so that the only difference between these two signals is the visual word form information. In the first group of contrasts, word-like stimuli (such as pseudowords) subtract the word form and the general visual information from the word stimuli (i.e., words–pseudowords), leaving only signal related to the word as a language unit. We will refer to this type of contrasts as "lexical" (LEX) contrasts. In the second type of contrast, perceptual stimuli (such as checkerboards) subtract the general visual information from the word stimuli signal (i.e., words–checkerboards), leaving the signal related to both the visual word form and the word as a language unit. We will refer to this type of contrasts as "perceptual" (PER) contrasts. These differences in functional signal can identify the different components and segregate word-responsive vOTC areas in the OTS. In this vein, we expect to find a more posterior OTS (pOTS) region (4) that is responsive to visual word forms, that should be detected only by PER contrasts. In addition, it is expected that the classical VWFA (4), which typically corresponds to the middle OTS (mOTS), will mainly be responsive to words as language units; hence, both LEX and PER contrasts should be able to locate this region. We speculate that the pOTS is associated with computations carried out by the visual system and that it is involved predominantly in visual feature extraction, while the mOTS is mainly involved in integrating information with regions along the

## Significance

**Understanding the function, structure, and connections of the ventral occipitotemporal cortex (vOTC) is critical to unravel the neural mechanisms determining how our brain accomplishes reading. Here, we identified two segregated areas along the vOTC posterior–anterior axis involved in two different aspects of visual word recognition: a posterior part responsible for visual feature extraction and an anterior part involved in integrating information from and to the language network. Converging evidence from functional, structural, microarchitectonic, and behavioral measurements consistently confirmed this posterior–anterior segregation in the vOTC and, importantly, revealed the pathways involved in different processes supporting reading.**

Author contributions: G.L.-U., M.C., and P.M.P.-A. designed research; G.L.-U. performed research; G.L.-U. and P.M.P.-A. analyzed data; and G.L.-U., M.C., and P.M.P.-A. wrote the paper.

The authors declare no conflict of interest.

This article is a PNAS Direct Submission.



Data deposition: Data and code related to this paper are available at https://www.bcbl.eu/Datasharing/PNAS2018Lermausabiaga/.

See Commentary on page 10542.

[1]To whom correspondence should be addressed. Email: garikoitz@gmail.com.

This article contains supporting information online at www.pnas.org/lookup/suppl/doi:10.1073/pnas.1803003115/-/DCSupplemental.

Published online September 17, 2018.

language network (14–16). It is also expected that the distinct pOTS and mOTS functional components will be differentially associated with reading behavioral indices from an independent lexical decision task including real words and consonant strings.

Structurally, it is accepted that both the gray-matter cells and their white-matter connections to other cortical structures support function. Therefore, in line with previous evidence (5, 8–13), we expect that the hypothesized pOTS and mOTS segregated vOTC regions are differently innervated by white-matter fiber tracts connecting them to distinct cortical areas involved in the visual word recognition process. In particular, we expected the pOTS to be connected to the intraparietal sulcus 0/1 segment (iPS) via the vertical occipital fasciculus (vOF) (17). Meanwhile, we expect the mOTS to be structurally connected to the language areas: to the supramarginal and angular gyrus regions in the posterior parietal cortex (pPC) through the posterior arcuate fasciculus (pAF) and to the inferior frontal gyrus (IFG) through the long segment of the arcuate fasciculus (AF) (9, 10). As the pAF and the AF share cortical endings in the vOTC, in the present work, we will focus on the pAF/vOF comparison due to the more clear separation of their vOTC cortical endings and the fact that they both structurally connect vOTC to parietal regions. Additionally, according to previous evidence showing cytoarchitectonic differences in the vOTC (12, 13, 18, 19), we expect to find supporting evidence for such segregation in the form of differences in the biological substrates of the gray-matter cells in pOTS and mOTS areas, as measured by T1 relaxation times. In line with evidence from previous studies that separately examined functional or structural segregations along the vOTC, the present work aims to further characterize the vOTC reading circuitry by using a multimodal approach combining functional MRI, structural MRI, and quantitative MRI (qMRI) as well as behavioral data.

## Results

**Two Functionally Segregated Regions in the vOTC.** Our functional results revealed that most of the vOTC was highly responsive to the word-fixation functional contrast. Furthermore, we observed a gradual posterior–anterior decrease in activation from $y = -35$ to $-102$ [$F(3, 174) \geq 171.84$, $P < 0.0001$], suggesting that distinct areas respond to different signals involved in visually recognizing words: the general visual information signal, the visual word-form signal, and the word-as-a-language-unit signal. Nevertheless, the word-fixation contrast does not discriminate these different components (see *SI Appendix* for a detailed characterization of the word-fixation functional contrast in the vOTC, and see Fig. 8 for the used left vOTC masks).

To further examine functionally differentiated areas within the vOTC, we carried out six functional contrasts that have been reported in previous research, organized into two groups: PER and LEX. The PER contrasts consisted of RW vs. checkerboards (CB), RW vs. scrambled words (SD), and RW vs. phase-scrambled words (PS). The LEX contrasts consisted of real words (RW) vs. pseudowords (PW), RW vs. consonant strings (CS), and RW vs. false fonts (FF). Our results revealed that all of the averaged global maxima (GMax) from these six functional contrasts lay along the OTS (Fig. 1*A*). As hypothesized, the averaged GMax of the PER contrasts were located within the posterior part of the OTS, in the vicinity of the previously described posterior VWFA (pVWFA) (4). The averages of the LEX contrasts (RWvsPW/CS/FF) were located within the middle part of the OTS, overlapping roughly with what has been reported in previous studies as the classical VWFA (cVWFA) [ref. 4; see *SI Appendix*, Table S1 for Montreal Neurological Institute (MNI) stereotactic mean coordinates of GMax T values].

To statistically examine whether the PER and LEX functional contrasts locate different parts of the cortex, we first performed a one-way, repeated-measures ANOVA, with one independent

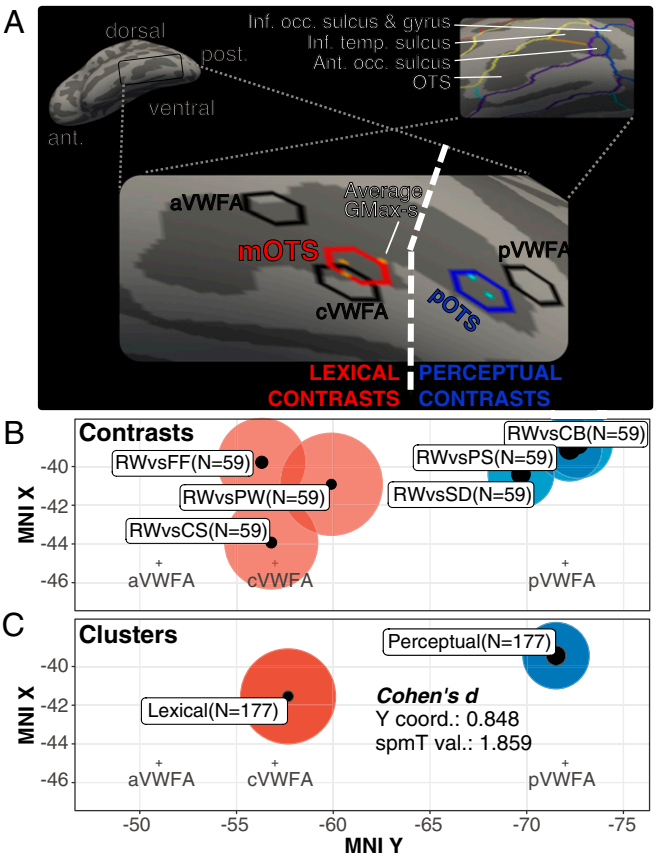


**Fig. 1.** Functional MRI contrasts. (*A*) OTS in Freesurfer's fsaverage left hemisphere inflated surface showing the averaged GMax for the LEX (RWvsCS/PW/FF) and PER (RWvsPS/CB/SD) contrasts. The red hexagon corresponds to the clustered LEX contrasts (mOTS), and the blue hexagon corresponds to the clustered PER contrasts (pOTS). The black hexagons correspond to VWFAs identified in previous research as aVWFA, cVWFA, and pVWFA and are drawn just for comparison purposes (4). (*B*) Functional activation results plotted in MNI152 *y* and *x* coordinates. The size of the inner black circle indicates the average T value, and the size of the colored outer circle is scaled to the standard deviation of the coordinate positions. Red outer circles are used for LEX contrasts, and blue outer circles are utilized for PER contrasts. (*C*) Analogous plot to *B* with clustered averaged values and standard deviations. The centers of the clusters define mOTS and pOTS. ant. occ. sulcus, anterior occipital sulcus; coord., coordinate; inf. occ. sulcus, inferior occipital sulcus; inf. temp. sulcus, inferior temporal sulcus; val., value.

measure, Contrast, that was manipulated over six levels (RWvsPW/CS/FF/PS/CB/SD), using the value of the Y MNI coordinate as the dependent measure. This analysis revealed a main effect of Contrast [$F(5, 290) = 15.72$, $P < 0.0001$, $R^2_{Adj} = 0.37$]. Simple-effect post hoc analysis showed systematic one-to-one statistically significant differences for contrasts belonging to the PER group vs. contrasts belonging to the LEX group [all $q \leq 0.005$, false discovery rate (FDR) corrected for multiple comparisons]: All LEX contrasts located areas anterior to those located by PER contrasts (Fig. 1*B*). No statistically significant differences emerged for comparisons involving functional contrasts within each of the PER or LEX contrast groups (all $q \geq 0.78$, FDR corrected). To examine the reproducibility and reliability over time of the main experiment results, these analyses were also conducted for a subset of participants who came back for a retest session after 7–10 d (test–retest Experiment; *Methods*). Test–retest analyses showed similar findings over time (*SI Appendix*).

Second, a hierarchical cluster analysis was conducted by using both the Y MNI coordinate and the averaged GMax T values as

dependent measures. The clustering algorithm, either using both variables at the same time or independently, separately grouped PER contrasts and LEX contrasts (Fig. 1*C*). These results confirmed the original allocation of the different contrasts to either the PER or LEX groups. Therefore, the clustered PER contrasts corresponded to the hypothesized pOTS and the clustered LEX contrasts to the mOTS. The effect sizes of the differences between the PER and LEX contrasts were calculated by using Cohen's *d* coefficients: *y* axis = 0.848; T value: 1.859.

Third, to further examine pOTS–mOTS segregation, we implemented an additional fMRI analysis using surface-based probabilistic maps, for the aggregated PER and LEX contrasts. We binarized the activations inside the OTS by using an individualized variable threshold, and with these binary values, we created a probabilistic map grouping all of the subjects' values. For the PER contrasts, the probabilistic maps showed two differentiated clusters overlapping with the previously identified pOTS and mOTS (Fig. 2*A*). In line with our hypothesis, these results indicated that the PER contrast signal contains the visual word-form signal, which activates the pOTS, and the word-as-a-language-unit signal, which activates the mOTS. For the LEX contrasts, the probabilistic map showed a cluster overlapping with the previously defined mOTS. This cluster extends to more anterior OTS areas, but not to posterior ones, in line with the general hypothesis that the LEX contrasts isolate lexical processes in more anterior OTS regions.

Finally, we conducted region-of-interest (ROI) parameter estimate analyses to examine the pattern of activation in the pOTS and mOTS regions for the PER and LEX group contrasts (Fig. 2*B*). Planned comparisons revealed an overall stronger recruitment of both pOTS and mOTS regions for PER vs. LEX contrasts [$t(55) = 0.67$, $P < 0.001$], while LEX contrasts showed significantly stronger engagement of the mOTS than pOTS [$t(55) = 0.18$, $P = 0.021$]. No statistically significant differences emerged in the recruitment of the mOTS and pOTS for the PER contrasts [$t(55) = 0.07$, $P = 0.351$].

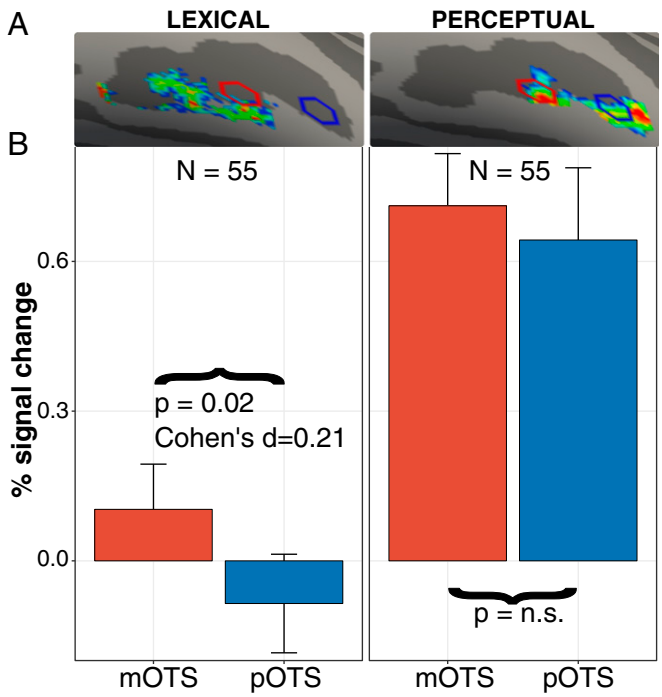


**Fig. 2.** Probabilistic maps for the aggregated LEX and PER contrasts in the OTS and parameter estimates (percentage signal change) analyses for the mOTS and pOTS. (*A*) The PER contrasts showed two activation clusters in the probabilistic maps which overlapped with the described mOTS and pOTS. LEX contrasts only showed anterior activated clusters in OTS. (*B*) PER contrasts revealed similar percentage signal change across both the mOTS and pOTS. For LEX contrasts, the mOTS was more strongly engaged than the pOTS. Error bars represent one SEM. n.s., not significant.

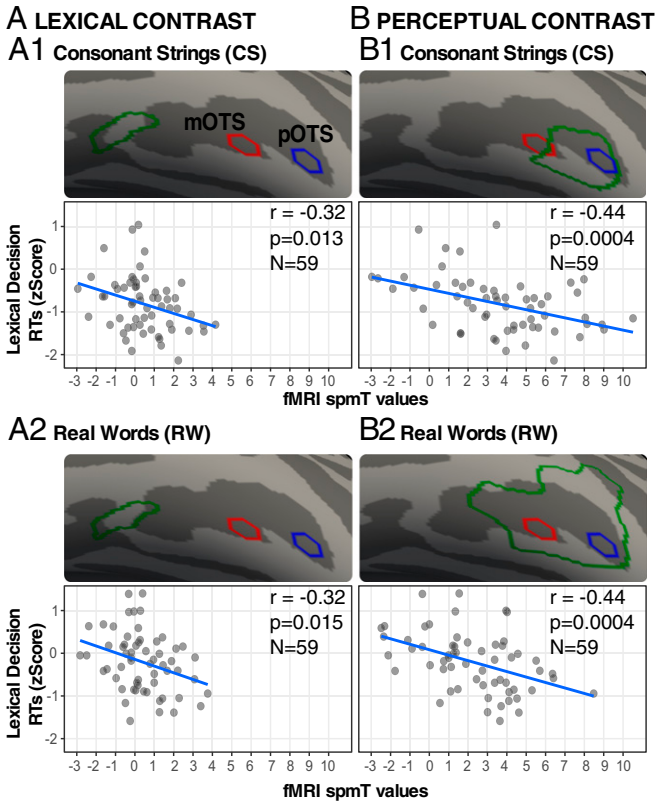


**Fig. 3.** Associations between functional activation and reading latencies. The green outlines show areas where significant associations between fMRI activation and reading behavior RTs (z scores) were found, vertex- and cluster-wise corrected for multiple comparisons ($P = 0.05$). (*A*) Associations between the aggregated LEX contrast fMRI activation with CS (*A1*) and RW (*A2*) RTs (z scores). (*B*) Cortical associations between aggregated PER contrasts fMRI activation with CS (*B1*) and RW (*B2*) RTs (z scores). The scatterplots show the averaged functional *t* values inside the green outlined regions (horizontal axis) against the behavioral indices RT *z* scores (vertical axis). The mOTS (red hexagon) and pOTS (blue hexagon) are rendered as references.

**Posterior and Anterior vOTC Regions Showed Different Functional-Reading Behavior Association Patterns.** Next, we tested whether individual reading abilities measured outside of the scanner were differentially associated with functional activations along the vOTC in our fMRI localizer task. To this end, we performed separate vertex-wise linear regression analyses restricted to the vOTC, using the averaged T values for the aggregated PER and LEX contrasts as independent variables and individual average reaction times (RTs) to CS and RW in a lexical decision task performed outside of the scanner as dependent variables. For the LEX contrasts, results revealed a single anterior OTS cluster associated with reading RTs across both CS and RW ($P = 0.01$; Fig. 3*A*). In contrast, for the PER contrasts, these brain-behavior association analyses revealed different functional clusters in the vOTC for reading CS and RW (Fig. 3*B*). For CS, the most significant functional cluster was observed in the most posterior part of the OTS ($P = 0.0004$), overlapping roughly with the pOTS. On the other hand, the most significant functional cluster associated with RW reading for the aggregated PER contrasts

was more extended ($P = 0.0004$), covering both the pOTS and mOTS. All of these statistically significant brain-behavior regressions were negative, indicating that stronger functional activation was associated with shorter reading latencies.

**Different Structural Connectivity Patterns in pOTS and mOTS.** In the previous sections, results consistently confirmed the identification of two segregated functional areas differentially associated with reading behavior: the pOTS and mOTS. To test the hypothesis of a structural segregation between these functional vOTC areas and the vOF and pAF white-matter tracts (Fig. 4*A*), we first calculated probabilistic maps for the cortical endings of the pAF (Fig. 4*B1*) and vOF fiber tracts (Fig. 4*B2*). To examine the number of cases where the cortical endings of the vOF and pAF corresponded to the pOTS and mOTS, McNemar $\chi^2$ tests were performed within the cortical endings of each of these fiber tracts. Within the cortical endings of the vOF, more cases were found to correspond to the pOTS (73%) than to the mOTS (46%), $\chi^2(59) = 10.23$, $P < 0.01$. In contrast, within the cortical endings of the pAF, more cases were found to correspond to the mOTS (31%) than to the pOTS (15%), $\chi^2(59) = 4.27$, $P < 0.05$. Interestingly, all of the PER functional contrasts lay posterior to the intersection (Fig. 4 *C1* and *C2*, where the contrast and cluster information is shown separately for the MNI *x*–*y* axes); in contrast, the LEX functional contrasts, although sparse, lay anterior to or within the intersection of the pAF and vOF.

Additionally, to further investigate the relation between the tracts' cortical endings and our previous PER and LEX functional contrasts results, we performed one-sided *t* tests comparing the average vertex-wise *t* values of the contrasts inside the cortical endings of the vOF and pAF white-matter tracts inside the vOTC. We predicted that the PER functional contrast would have higher vertex-wise average *t* values in the vOF relative to the pAF and that, in contrast, the LEX functional contrasts would have lower vertex-wise average *t* values in the vOF than in the pAF. These *t* tests for both the PER [$t(59) = 4.80$, $P < 0.0001$] and LEX [$t(59) = -1.99$, $P = 0.026$] contrasts were significant, confirming our predictions.

In sum, these results revealed a strong correspondence between functional and structural segregations of anterior and posterior vOTC regions. Functional locations of the PER contrasts and their activation levels overlapped with those observed for the vOF fiber tract cortical endings. Similarly, functional locations of LEX contrasts and their activation levels corresponded to those observed for the pAF white-matter tract cortical endings.

**Cytoarchitectonic-Related Differences in pOTS and mOTS.** Previous functional and cytoarchitectonic research evidence suggested regional segregations along the posterior–anterior and lateral–medial axes of the vOTC (11–13, 18, 19). More precisely, the lateral–medial segregation would correspond to different specializations within the fusiform gyrus (FG): The FG1 and FG3 areas are more medial and functionally dedicated to places; the FG2 and FG4 areas are more lateral and functionally dedicated to faces and words. In contrast, the posterior–anterior segregation within the FG would correspond to different hierarchical transformations. The FG1 and FG2 areas are located more posteriorly, and they are a hierarchically anterior step to FG3 and FG4 in their corresponding specialized process. Based on this evidence and the position of these FG regions, we hypothesized that our functionally defined pOTS and mOTS would be strongly associated with the FG2 and FG4 areas, respectively. In Fig. 5*A*, we superimposed our functional results (pOTS and mOTS) and the vOF and pAF cortical tract ending probabilistic maps with the cytoarchitectonic areas FG2 and FG4 (13), where it can be seen how well the intersection of the vOF and pAF cortical tract endings corresponds to the intersection between

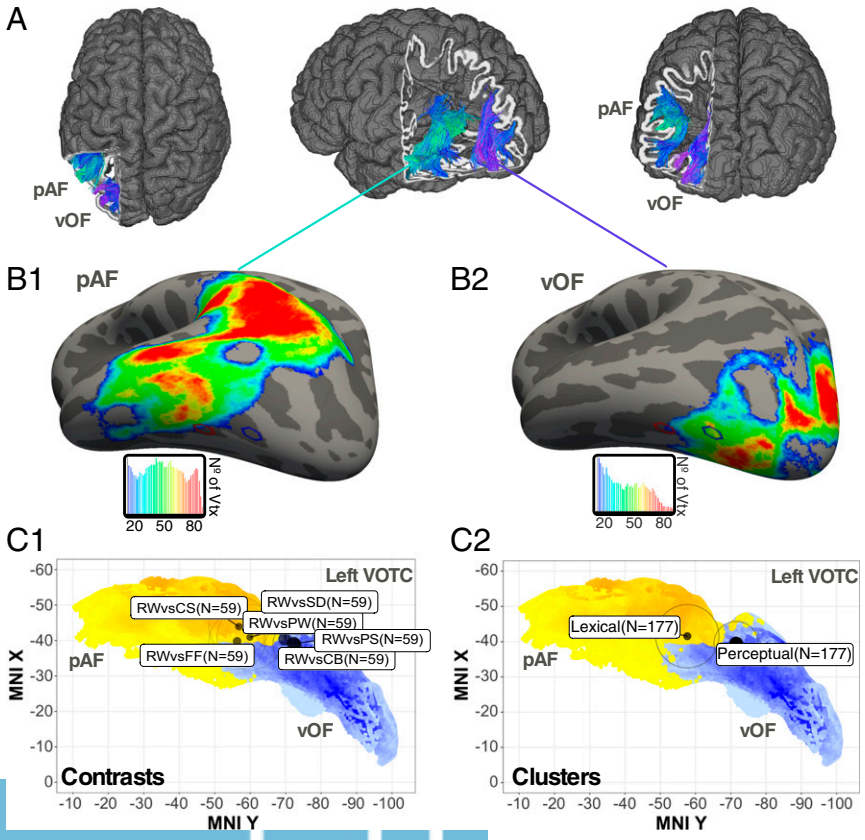


**Fig. 4.** Associations between functional activations and the cortical endings of the tracts of interest. (*A*) A 3D representation of the pAF and vOF tracts for the left hemisphere of a representative subject, in standard axial, sagittal, and coronal views. (*B*) Average inflated surface rendering probabilistic maps (thresholded at 20%) of the pAF (*B1*) and vOF (*B2*) tract cortical endings in the vOTC cortex. In the probabilistic map, red indicates that a high percentage of subjects showed a correspondence between the tract and that vertex, green indicates medium correspondence, and blue indicates low correspondence. Note the outlines of the mOTS (red) and pOTS (blue) superimposed: The mOTS corresponds to the pAF cortical endings and the intersection of the cortical endings of both tracts, and the pOTS overlaps with the cortical endings of the vOF. (*C*) The same white-matter cortical endings from *B*, but projected into MNI *x* and *y* axes, with pAF in yellow and vOF in blue. Both graphs in *C* show the same projections, but they overlay specific (*C1*) and clustered (*C2*) contrasts (the LEX cluster defines the mOTS and the PER cluster the pOTS). The size of the inner black circle indicates the average *t* value, and the size of the outer circle is scaled to the standard deviation of the coordinate positions.

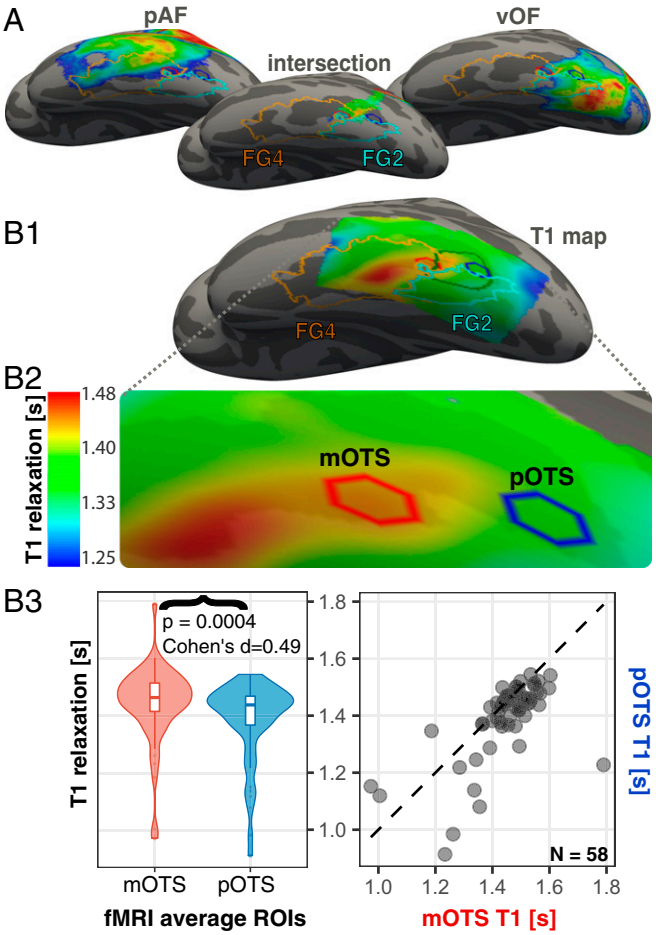


**Fig. 5.** White-matter cortical endings and T1 relaxation time results on the left OTS. (*A*) pAF, vOF, and the intersection of the cortical ending probabilistic maps on the left hemisphere. The red hexagon corresponds to mOTS, and the blue hexagon corresponds to pOTS. The orange outline corresponds to the cytoarchitectonic area FG4, and the light blue outline to cytoarchitectonic area FG2 (13). The intersection of the pAF and vOF cortical tract endings roughly coincides with the separation between FG2 and FG4 cytoarchitectonic areas. *B1* shows the same mOTS, pOTS, FG2, and FG4 area outlines, with an additional green outline corresponding to the cluster of significant association between the averaged PER contrasts fMRI T values, and the reading behavior index (CS detection RTs in the lexical decision task). The heatmap corresponds to the T1 relaxation values, which can be seen enlarged in *B2*. (*B3*) Comparison of T1 relaxation times in mOTS and pOTS: *Left* shows violin plots representing the different T1 relaxation values in each ROI, and the significance and effect size of a simple *t* test between these values; *Right* shows a scatterplot with the individual subject values in pOTS plotted against the equivalent mOTS values. Almost all values systematically lie below the identity line, and the T1 relaxation values of the mOTS and pOTS show a highly predictable relation.

these cytoarchitectonic FG areas. Additionally, to examine the association of the functionally defined pOTS and mOTS with these two cytoarchitectonic areas, we created an averaged T1 relaxation time map of the OTS to further study gray-matter microarchitectonic properties. Fig. 5*B1* shows a triple overlap with convergent results: (*i*) mOTS corresponds to the FG4 area and, although slightly off, pOTS corresponds to the FG2 area; (*ii*) pOTS shows low T1 values and mOTS exhibits high T1 values (Fig. 5*B2*); and (*iii*) higher T1 values are related to the FG4 area relative to the FG2 area, and there is an increasing gradient in T1 values going from posterior-to-anterior OTS.

To statistically check the differences observed in Fig. 5*B2*, we compared the averaged T1 values in the pOTS and mOTS and observed a significant difference ($P < 0.0004$) with the pOTS showing lower T1 values relative to the mOTS (see violin plot in Fig. 5*B3*). The scatterplot in Fig. 5*B3* shows that the pOTS T1 value is lower than the mOTS T1 value for most subjects.

## Discussion

The goal of the present study was to systematically investigate segregations in OTS regions by using a multimodal approach combining functional, structural connectivity, and cytoarchitectonic-related MRI indices along with behavioral reading measures. Accurate parcellation should help to elucidate the neural pathways and mechanisms governing visual word recognition. Our results revealed that (*i*) there are two functionally segregated areas within the OTS, a posterior and a middle region; (*ii*) these areas are associated with different long-range projections, with pOTS probably projecting to the iPS via the vOF and mOTS likely projecting to the angular gyrus, via the pAF, and to the IFG, via the long segment of the AF; (*iii*) reading behavior is associated with functional activation in these segregated OTS regions; and (*iv*) these OTS regions have different T1 values, supporting previous evidence regarding their cytoarchitectonic properties (*SI Appendix*, Fig. S3 represents a graphical abstract integrating all of the main results reported in this work).

**Two Functionally Segregated Areas Within the OTS.** In recent years, extensive research devoted to investigating the VWFA has made important advances at the empirical and conceptual levels, revealing the involvement of the OTS in word recognition across different experimental settings and designs and generating critical theoretical accounts regarding the role of vOTC. However, the considerable variation across studies regarding the specific location of regions involved in word recognition-related processes has made it highly desirable to further divide the OTS area into subregions that may be involved in more specific responses. By using a systematic hypothesis-driven approach, results from the present study reveal two functionally segregated regions (i.e., pOTS and mOTS) linked to previous vOTC locations reported in the literature and provide insight into the location discrepancies observed in previous studies. Fig. 6 summarizes our results showing SPM *t* values in each vertex along the posterior–anterior *y* axis for the averaged PER (in red) and LEX (in cyan) contrasts across subjects and *x*–*z* coordinates. Since both PER and LEX contrasts include linguistic information about the word, the main difference (in Fig. 6, the two-headed gray arrows) between them relates to the vOTC response to visual word forms.

Whereas the response signal to the PER contrasts decreases along the *y* axis coordinates (from the pOTS to the mOTS), the response signal to the LEX contrasts increases. The fact that the area along the mOTS is responsive to linguistic information is confirmed by LEX contrasts showing their maxima along the mOTS area coordinates, which correspond to the cVWFA described in previous research (4, 20–23). Similarly, evidence from studies on auditory word recognition has revealed that spoken words recruit the area corresponding to the mOTS (24, 25),* illustrating that the cVWFA/mOTS is indeed responsive to word forms and to orthographic and lexical processes; however, this is not the case for the pOTS, which appears to be responsive only to low-level visual information, which roughly corresponds to the pVWFA described in previous studies (4, 26, 27). Interestingly, this dissociation in the VWFA may reconcile two views on the kind of computations performed by the VWFA and how

*Planton S, et al., Involvement of the visuo-orthographic system during spoken sentence processing. Cognitive Neuroscience Society 24th Annual Meeting, March 25–28, 2017, San Francisco.

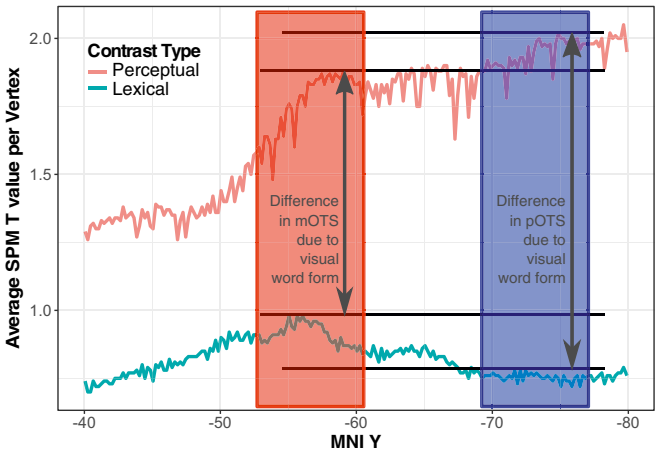


**Fig. 6.** Averaged T values in each vertex plotted along the *y* axis for averaged PER (red) and LEX (cyan) functional contrasts across subjects and *x*–*z* locations. The red box represents the location of the mOTS and the blue box the location of the pOTS. The horizontal parallel black lines indicate the maxima inside the pOTS and mOTS for the PER and LEX averaged functional contrasts. Thus, the gray two-headed arrows indicate the difference of response in the pOTS and mOTS due to visual word form signal.

information flows into the VWFA: bottom-up vs. top-down (16, 28). While pOTS may be activated mostly by bottom-up information flow, mOTS may receive both bottom-up and top-down information.

Importantly, the fact that such a long strip of the vOTC, stretching from the pOTS to the mOTS, is responsive to visual word forms, may also explain the variability in location results from previous studies. Indeed, two different studies aiming to examine linguistic effects could localize the functional signal responsive to visual word forms in anterior, as well as in posterior regions along the vOTC, depending on the functional contrasts of choice. Moreover, intersubject variability in the location of these regions might have played a role in previous studies and in further characterizing the specific role of different vOTC subregions. In this vein, previous studies have highlighted the importance of defining responsive regions along the vOTC at the individual level rather than only at the group level (3, 29). Thus, using a systematic approach in terms of the functional contrasts utilized to localize different regions within the vOTC and examining functional data at the individual level are critical methodological issues that should be taken into account. Additionally, despite previous evidence from studies separately examining functional or structural segregations along the vOTC (4, 5, 7–13), it is crucial to combine both functional and structural data to further understand the pathways used to transfer information derived from the functional computations carried out in different vOTC subregions, since they are intrinsically related.

Brain-reading behavior associations revealed that functional activation for the PER contrasts correlated with RTs for correctly identifying CS, but only in the pOTS. Correctly identifying CS as nonwords is basically a perceptual task, since we cannot read CS, and a rapid visual scan can detect them due to the lack of vowels. In contrast, when using the RTs of correctly identified RW as the behavioral index, significant associations were observed with PER contrasts along the entire OTS, including both the pOTS and mOTS. The pOTS association with RW is consistent with our previous result (the word form part of reading a word), meanwhile the mOTS association with RW is consistent with the functional findings regarding its role in processing lexical information. In sum, word-form processing for both CS and RW was associated with pOTS PER contrast activations, but the lexical information processing (only present in RW) was associated with both the pOTS and mOTS PER contrast activation, suggesting that it is necessary to access the language network to discriminate RW. This finding is consistent with our functional results and previous evidence.

**Different Functional Areas Supported by Different White- and Gray-Matter Structures.** Although previous research has specifically characterized vOTC regions at the structural level (5, 8–10, 13, 17, 30–32), no previous studies have systematically linked function and structure during visual word-recognition processes. The present study showed that diffusion and quantitative structural measures consistently find that the functionally identified pOTS and mOTS areas are associated with different white-matter tracts and gray-matter substrates. On the one hand, the pOTS seems to be structurally connected to the iPS via the vOF, suggesting that this functional region mainly carries out occipital computations at this stage of visual word processing. Kay and Yeatman (17) showed the same functional and structural connectivity pattern between the iPS and the vOTC. Furthermore, they showed that top-down processes involved in high-level reading tasks can modulate responses in the vOTC (see also ref. 33). In order not to impose external manipulations and avoid the iPS top-down effects, this study used a low-level reading task (see *Methods* for further details).

On the other hand, our findings revealed that the mOTS is associated with the cortical endings of the pAF (and, hence, of the long segment of the AF). Therefore, we consider that the mOTS might be the gateway connecting structurally the vOTC circuit to other regions along the language network: to the angular and the supramarginal gyri likely through the pAF and to the IFG probably via the long segment of the AF. This result suggests that the mOTS is the region where the integration between the output from the visual system and the language network takes place.

Additionally, qMRI data analyses consistently revealed different gray-matter substrates in the functionally identified pOTS and mOTS areas. Finding different T1 relaxation time values can be multidetermined due to the fact that T1 relaxation time in gray matter depends on the density of the macromolecules, such as contained in the cell walls present in the voxels and the composition of lipids. Although the pOTS seems to lie in the vicinity of the probabilistic FG2 region, our results showing lower T1 relaxation values in the pOTS than in the mOTS regions are highly consistent with those from the Weiner et al. (13) cytoarchitectonic study revealing that the FG2 presents more densely packed neurons in layer IV than the FG4. In fact, the mOTS overlaps with the probabilistic FG4 region.

Similarly, in a previous study combining MRI and quantitative cytological analysis of the FG, Schenker-Ahmed and Annese (19) found that posterior FG regions thought to be involved in the processing of features at the local level tended to show smaller and more tightly packed neurons. In contrast, the neurons appeared to be larger and sparser in anterior FG regions, where greater integration of information is thought to be required. These findings concur with the evidence obtained from our study and previous evidence suggesting that the posterior vOTC is involved in detail-oriented data processing, while more anterior parts perform more abstract processing and integrate information from other cortical areas (15). Nevertheless, it is not currently possible to precisely and unequivocally relate T1 relaxation values in the pOTS and mOTS with cytoarchitectonic FG regions, since these are measures obtained by using rather different procedures.

Thus, the present study showed that functional segregations were also supported by consistent structural differences. It is hoped that future research will also incorporate more precise VWFA localizations, combining both functional and structural localizers. In fact, it might be possible to predict where differences

in functional activation will occur by combining refined structural techniques. Interestingly, it has already been suggested that the brain might be prewired for reading (34, 35), because it is possible to predict from the structural connectivity pattern in prereaders where the VWFA will lie once toddlers have learned to read (5).

**Visual Feature Extraction and Integration with the Language Network.** The results from the present study suggest that the pOTS plays a critical role in visual feature extraction and that only when the signal gradually reaches the mOTS is the information derived from the functional computations of this region transferred and/or integrated with other regions along the language network, possibly through the pAF and the long segment of the AF. Nevertheless, our data cannot determine whether these regions are involved (*i*) in bottom-up only (*ii*) or in interactive bottom-up and top-down processes, as stated by two of the main theoretical proposals regarding the functional role of this region (16, 28).

First, regarding pOTS, our results cannot confirm if words per se can be recognized in the pOTS (28) or if the participation of the mOTS is strictly necessary for this (16). There is evidence, however, suggesting that shapes that conform to words are recognized through a perceptual learning process (14, 36, 37) in regions overlapping with the pOTS and even in more posterior visual areas. Our findings align well with this previous evidence, showing areas that are highly responsive to word forms in the pOTS. This suggests that this area may be necessary for visual word recognition. However, further research should determine to what extent the pOTS is sufficient for recognizing words.

Second, if the mOTS region is only involved in bottom-up processes, then it should be recruited to transfer information about the already recognized word to the language network only when a word is seen. However, the mOTS is also functionally recruited when words (24, 25)[†] are heard. This casts serious doubts on the claim that this area only processes bottom-up visual information, unless simultaneous functional activations in the mOTS occur because of existing connectivity needed for bottom-up processes. However, this possibility seems unlikely. In our view, the mOTS is involved in interactive bottom-up and top-down processes, integrating feed-forward and -backward information from and for regions along the language network, which are required for actual word recognition.

Acknowledging what is known about redundancy in the brain (16, 38, 39), it seems quite plausible that an interactive and redundant mechanism is in place for visual word recognition. Even if the pOTS and more posterior areas can become independently trained for recognizing words, there should be a feed-backward loop from the language system into anterior vOTC areas to integrate information and verify reading processes. Also, although perceptual learning might be important for speeding up reading processes, this specific ability does not need to be in place when, for instance, we read very-low-frequency words. In our view, the predominant theoretical debate around bottom-up and top-down processes in the vOTC partially stems from intrinsic limitations in the techniques employed and a lack of precise individual and structurally informed cortical localizations. Basically, both pOTS and mOTS are responsive to visual word forms, but each region may represent a distinct hierarchical step, perform different but complementary computations, and is involved in transferring and integrating information with different visual and reading regions along the language network to achieve reading.

Importantly, diverging from previous studies showing a gradient of activation along the posterior-to-anterior vOTC axis (7, 40–42), our results consistently showed two functionally and structurally segregated areas within the vOTC. Although the gradient along the vOTC *y* axis observed in previous research may perfectly hold as a result of certain analytical approaches (Fig. 6), and it also makes good neurobiological sense considering that single regions do not work in isolation, the multimodal approach carried out in the present study has been critical to further elucidate these two salient foci within the vOTC circuit and their distinct functional roles, structural connectivity, and gray-matter microarchitectonic properties. In this vein, the present study paves the road for further research to examine the differential involvement of the pOTS for reading manipulations posing stronger visual demands and the mOTS for reading manipulations further taxing interactions with the extended language network. As previously indicated, whereas the pOTS seems to correspond to the area identified as the pVWFA (4, 43, 44) or the pOTS (13, 26, 27, 45) in previous studies, the region here defined as mOTS corresponds to a region that has classically been identified as the VWFA. This region falls close to the coordinates proposed in work by Cohen and Dehaene as well as the averaged results obtained in the meta-analysis of Jobard et al. (46).

Finally, two limitations should be noted. First, all of the analyses performed in the present work were circumscribed to the left hemisphere. Future research or reanalysis of the present dataset focused on the right hemisphere might help to further understand to what extend the observed posterior-to-anterior segregation is specific to the left but not the right vOTC. In line with previous evidence, it would be reasonable to expect that, whereas the pOTS can be similarly identified in the right hemisphere, this might not be the case for the mOTS. Second, our functional probabilistic analysis, brain-behavior regressions, and T1 relaxation times showed some regions more anterior to the mOTS that, although they did not overlap with each other, can be related to some extent to the anterior VWFA (aVWFA) identified in previous studies. However, in the present work, the functional signal obtained along those anterior regions was considerably weaker than the one observed for the main pOTS and mOTS regions (Fig. 6). Future studies specifically designed to examine this region can shed further light on its functional involvement in lexical reading processes that require further interactions with the language network and, possibly, its structural connections with this network via the pAF and/or the long segment of the AF.

In conclusion, the present study provides the strongest converging functional, structural and behavioral evidence to date for the segregation of visual word recognition processes in the vOTC. Our data supports the existence of a pOTS region, responsible for visual feature extraction, structurally connected to the intraparietal sulcus via the vOF, and a mOTS region, responsible for integrating information with regions along the language network, structurally connected to the angular gyrus via the pAF and to the IFG through the long segment of the AF. In addition to the differences in functional activation and white-matter connectivity, our results revealed fundamental differences in the gray-matter microarchitecture supporting this segregation within the vOTC.

## Methods

**Participants.** A total of 66 different undergraduate students participated in the study. Thirty-one of them also participated in a second identical session separated by 7–10 d. Therefore, these data were divided into two experiments: the main experiment (age 24.31 ± 3.70 y; 40 females) and the test–retest experiment (age 24.34 ± 2.96 y; 17 females). For the main experiment, first-day acquisition sessions from the 66 unique participants were used. For the test–retest experiment, only those 31 participants that had participated in two acquisition sessions (first and second day) were selected. Data from three additional participants were excluded from further analysis due to incidental findings or technical problems with data acquisition.

All participants were right-handed healthy young adults, with no history of psychiatric, neurological, attention, or learning disorders, and with normal or corrected-to-normal vision, and all of them gave written informed consent. The

[†]Planton S, et al., Involvement of the visuo-orthographic system during spoken sentence processing. Cognitive Neuroscience Society 24th Annual Meeting, March 25–28, 2017, San Francisco.

experiment was approved by the BCBL Ethics Review Board and complied with the guidelines of the Helsinki Declaration. Furthermore, all participants completed an intelligence test [using the Kaufman Brief Intelligence Test, 2nd edition; KBIT-2 (47)]; and an objective measure of vocabulary, which is an adaptation of the Boston Naming Test (48) that controls for cognates in Spanish, Basque, and English. All participants were highly proficient in Spanish.

**Materials and Experimental Procedure.** Participants performed a block design functional localizer in the scanner. Before they underwent MRI scanning, they practiced a behavioral version of the fMRI experiment and were instructed to pay attention to the different visual stimuli that would be presented to them and to provide manual responses to the task stimuli (i.e., items framed with a black rectangle). The fMRI localizer stimuli were presented in black at the center of the screen against a gray background (RGB = 128, 128, 128; Fig. 7, *i–vii*) and were organized into eight experimental conditions and one task condition. The task condition (Fig. 7, t1) used stimuli from the seven main conditions. As soon as a black rectangle appeared framing the stimulus, participants were instructed to press a button. Two full sets of stimuli were designed, with a total of 80 stimuli per condition and per set [except for the RW condition with 160; see below]. These sets were counterbalanced across subjects. Next, we describe the materials used in each of the seven main experimental conditions: (*i*) RW: 4-to-6 letter Spanish words selected from the EsPal database (49) with high frequencies ranging from 50 to 500 (RWH) and low frequencies ranging from 0.5 to 5 (RLEX). Since most of the participants were Spanish–Basque bilinguals, words were checked for cross-language cognates in Basque by using the E-Hitz database (50). We also used an algorithm for the stochastic optimization of stimuli (51) to create two definitive counterbalanced sets of 160-word lists (comprising 80 RWH and 80 RLEX), equating them in terms of frequency, number of letters, bigram frequency, concreteness, and number of neighbors. For this experiment, we combined both RLEX and RWH in a unique RW group. (*ii*) PW: generated using the Wuggy tool (52) on a pool of words comprising 50% randomly selected from RWH and 50% randomly selected from RLEX. (*iii*) CS: generated by substituting all vowels in the PW with random consonants to equate their length to the other stimuli. (*iv*) PS: generated by shifting the word image in the frequency domain (26), using the tools provided by the Stanford Vistasoft package (https://github.com/vistalab/vistasoft/wiki) on a pool of words comprising 50% randomly selected from RWH and 50% randomly selected from RLEX. (*v*) SD: designed by creating 10 × 10 pixel tiles and mixing them randomly, using words from a pool comprising 50% randomly selected from RWH and 50% randomly selected from RLEX. (*vi*) CB: consisting of 15 pixel size black and white squares, with a length equated to the length of RW. (*vii*) FF: Georgian was used as the letter system of choice to produce FF, with a letter-by-letter translation. Participants were asked if they were familiar with the Georgian script before they took part in the experiment. FF were generated using words from a pool comprising 50% randomly selected from RWH and 50% randomly selected from RLEX.

After MRI data acquisition, a lexical decision task was administered to participants to obtain behavioral measures (i.e., accuracy and RTs) of their abilities to discern between real words, pseudowords, and consonant strings. The set of stimuli that had not been used for the fMRI localizer was used for the lexical decision task.

**MRI Data Acquisition.** Participants were scanned in a 3T Siemens TRIO whole-body MRI scanner (Siemens Medical Solutions), using a 32-channel head coil. Headphones (MR Confon) were used to dampen background scanner noise and to enable communication with experimenters while in the scanner. To limit head movement, the area between participants' heads and the coil was padded with foam, and participants were asked to remain as still as possible.
***Structural.*** T1-weighted images were acquired with a multiecho (ME) MPRAGE sequence with TE-s = 1.64, 3.5, 5.36, and 7.22 ms, TR = 2,530 ms, FA = 7°, field of view (FoV) = 256 × 256 mm, 176 slices, and voxel size = 1 $mm^3$. Additionally, a T2-weighted sequence was acquired with TE-s = 425 ms, TR = 3,200 ms, FoV= 256 × 256 mm, 176 slices, and voxel size = 1 $mm^3$.

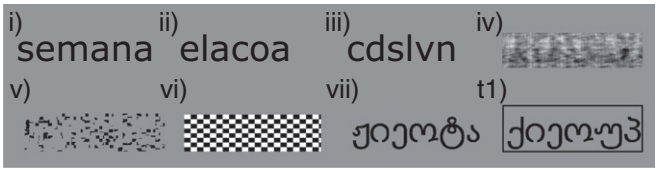


**Fig. 7.** Examples of stimuli for the seven experimental conditions and the task included in the functional localizers. (*i*) RW. (*ii*) PW. (*iii*) CS. (*iv*) PS. (*v*) SD. (*vi*) CB. (*vii*) FF. (*t1*) Example of task stimuli.

Diffusion-weighted images (DWIs) were acquired in three different sequences. The first two sequences had 30 directions (with a *b* of 1,000 s/$mm^2$) and 60 directions (with a *b* of 2,500 s/$mm^2$), respectively. These two sequences had five interleaved *b0*-s and A >> P phase encoding direction. The third sequence was acquired with six *b0*-s using the opposite phase encoding direction *P* >> A, and it was used for spatial distortion compensation. These three sequences were acquired by using the following parameters—TR = 6,766 ms, TE = 110 ms, FA = 90°, isotropic 1.8 $mm^3$ voxel size, 78 slices with 0% gap—and were acquired with a multiband acceleration factor of 2.

qMRI measurements were obtained from the protocols set forth in ref. 53. T1 relaxation times were measured from four T1-flash images with flip angles (FAs) of 4°, 10°, 20°, and 30° (TR = 12 ms, TE = 2.27 ms) at a scan resolution of 1 $mm^3$. For the purposes of removing field inhomogeneities, we collected four additional spin-echo inversion recovery (SEIR) scans with an echo-planar imaging (EPI) readout, a slab inversion pulse, spectral spatial fat suppression, 2× acceleration factor, and a TR of 3 s. The inversion times were 50; 400; 1,200; and 2,400 ms, and were collected at a 2 × 2 mm in-plane resolution and a slice thickness of 4 mm.
***Functional.*** Images were acquired by using the same gradient-echo echo-planar pulse sequence with the following acquisition parameters: TR = 24,00 ms, time echo (TE) = 24 ms, 47 contiguous 2.5 $mm^3$ axial slices, 10% interslice gap, FA = 90°, and FoV = 200 × 200 mm. Before each scan, four volumes were discarded to allow for T1-equilibration effects. Participants viewed stimuli back-projected onto a screen by a mirror mounted on the head coil. For these functional tasks, participants were provided with a response pad.

The localizer consisted of two separate functional runs, each run consisting of two activation blocks per condition and rest fixation blocks that were interleaved with activation blocks. Activation blocks lasted 12 s and included 20 stimuli of the same condition, each presented for 400 ms and followed by a 200-ms blank space. Rest fixation blocks lasted 16.8 s to allow for the hemodynamic response function (HRF) to return to baseline before presenting the next activation block. Thus, four stimuli of the same condition were presented every 2.4 s (study TR). At the end of some blocks (randomized), one or two additional images were added for the perceptual task condition (Fig. 7, t1). In this task condition participants were asked to press a button when a rectangle appeared around a regular stimulus. The task condition was modeled separately in the general linear models (GLMs) and not taken into consideration in subsequent analyses. For the test–retest experiment, acquisition sessions were separated by 7–10 d to both minimize structural changes and avoid habituation.

**MRI Data Processing.**
***Structural.*** First, by using Vistasoft and a custom MATLAB script, all T1-weighted images were aligned along the ac–pc line and the midsagittal plane. These aligned T1s were used for the Freesurfer (54) pipeline along with the participants' corresponding T2-weighted images, which further helps to inform the skull stripping process. The Freesurfer pipeline performs the volumetric gray- and white-matter segmentations, providing several automated cortical parcellations that can be used in subsequent analyses and, additionally, converts the gray matter into a 2D mesh that can be used to display, visualize, and analyze information. For both volumetric and surface images, Freesurfer also provides an averaged brain in MNI305 space that can be used to compare and visualize individual subject information.

For DWI data, subject motion was initially corrected by coregistering each volume to the average of the nondiffusion weighted *b0* images (and gradient directions were adjusted to account for this coregistration). Using FSL's topup, the susceptibility induced off-resonance field was estimated, and eddy currents were corrected by using FSL's eddy tool (55). The *b* = 1,000 and *b* = 2,500 measurements were used to estimate fiber orientation distribution functions for each voxel using mrtrix3's multitissue constrained spherical deconvolution (56) (lmax = 4), and Freesurfer was used to inform the algorithm about the different types of tissues. Fiber tracts were estimated by using probabilistic tractography (with 500,000 fibers) using the iFOD2 algorithm (57). For each subject, the vOF and pAF were identified by using tools from the AFQ analysis pipeline (10, 58). By using Vistasoft, Freesurfer's mri_vol2surf, and custom scripts, the end-points of these tracts in the cortex were identified and separated into two different groups—vOF and pAF endings in vOTC and those ending outside of vOTC—to create the vOTC_vOF and vOTC_pAF ROIs. For the vol2surf transformation, the voxels were matched with the surface 1 mm below the cortical surface. DWI data are not reliable for gray matter, so it is usually advisable to do the matching in white matter, right below the areas of interest. Nevertheless, tract information is usually stronger in the sulci and is typically lost in the gyri. We see this as a limitation of the technique, not a characteristic of the brain.

qMRI data were processed by using the mrQ software package in MATLAB to produce the MTV and T1 maps. The mrQ analysis pipeline corrects for RF coil bias using SEIR-EPI scans, producing accurate proton density and T1 fits across the brain. By using individual participants' voxels containing CSF within the ventricles, maps of MTV are produced calculating the fraction of a voxel that is nonwater (CSF voxels are taken to be nearly 100% water). The full analysis pipeline and its description can be found at https://github.com/mezera/mrQ. The resulting individual T1 and MTV map images were translated to the individual cortical surface by using Freesurfer's mri_vol2surf function, and then, by using mri_surf2surf, all images were translated to the fsaverage space for intersubject comparison.

***Functional.*** For fMRI analysis, we used standard SPM8 preprocessing routines. First, slice timing was performed on every functional scan. Then, realignment for motion correction and 4-mm smoothing and volume repair using ArtRepair5 (59) was applied to the images. In the last stage of preprocessing, all of the functional images were coregistered to the ac–pc aligned anatomical T1-weighted image and resliced from the original 2.5 $mm^3$ voxels to the 1 $mm^3$ voxels in anatomical space. Thus, all functional images were in the same space as the individual anatomical images so that the ROIs from Freesurfer could be used without further modifications. Note that the images were not normalized to the standard MNI152 template.

Statistical analyses were performed on individual subject space by using the GLM. fMRI time series data were modeled as a series of impulses convolved with a canonical HRF. The motion parameters for translation (i.e., *x*, *y*, and *z*) and rotation (i.e., yaw, pitch, and roll) were included as covariates of noninterest in the GLM. Each block was modeled as an epoch of 12 s, time-locked to the beginning of the presentation of the first stimuli within each block. The resulting functions were used as covariates in a GLM, along with a basic set of cosine functions that high-pass-filtered the data, and a covariate for session effects. The least-squares parameter estimates of the height of the best-fitting canonical HRF for each study condition were used in pairwise contrasts. The functional volumes associated with the task conditions were modeled separately and were not taken into consideration in subsequent analyses.

The resulting individual T-map images (one per subject and contrast) were translated to the individual cortical surface by using Freesurfer's mri_vol2surf function, and then by using mri_surf2surf, all images were translated to the fsaverage space for intersubject comparison. By using a custom MATLAB script, all GMax values were obtained per each subject, contrast, and design, and the data were converted to MNI152 coordinates by multiplying with an affine transformation matrix for further analysis and comparison with the literature. Finally, we thresholded the T values to capture GMax $\geq$ 1.65, which corresponds to a $P \leq 0.05$.

**MRI Data Analyses.**

***Regional definition.*** From Freesurfer's automated aparc parcellation, we extracted one extensive cortical area of interest to be used as a mask in subsequent fMRI analyses. This cortical area covered the entire vOTC region and was constructed by including the FG, inferior temporal, and lateral occipital cortical regions from the aparc parcellation. As the response to words in the primary visual cortex was not part of this study, regions V1 and V2 were excluded from this mask. Values on the *y* axis less than or equal to −30 in the MNI152 space were also excluded from this mask (Fig. 8 *A* and *B*).

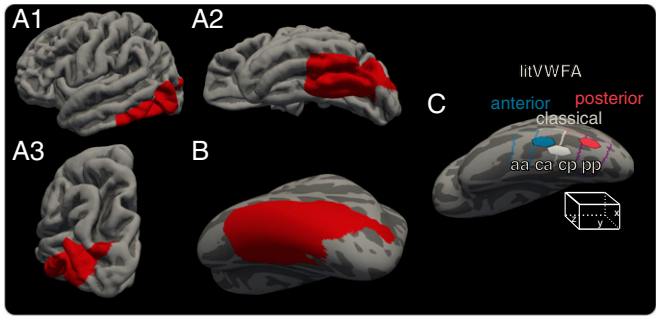


**Fig. 8.** Left vOTC area of interest (in red) used as a mask in the fMRI analysis and regional subdivisions within the vOTC. (*A*) Left hemisphere pial surface renderings in lateral (*A1*), ventral (*A2*), and posterior (*A3*) perspectives. (*B*) Left vOTC on an inflated Freesurfer fsaverage brain, with dark areas indicating sulci and light areas indicating gyri. (*C*) Regional subdivisions within the left vOTC area of interest. The litVWFA comprises three regions described in the literature: aVWFA, cVWFA, and pVWFA. The other four regions in aa-ca-cp-pp were manually designed to cover the litVWFA region and the OTS without overlaps or empty spaces between them. They were organized along an anterior–posterior gradient.

To further characterize the functional activations and structural differences in our main vOTC area of interest, we also created two different sets of regions named litVWFA and aa-ca-cp-pp within the vOTC (see Fig. 8*C* and definitions below). As the name suggests, the litVWFA set comprises three regions based on published coordinates in the literature (4, 43), called aVWFA, cVWFA, and pVWFA. The coordinates for the center-points of these areas were: aVWFA (Talairach: −43, −48, −12; MNI152: −45, −51, −12), cVWFA (Talairach: −43, −54, −12; MNI152: −45, −57, −12), and pVWFA (Talairach: −43, −68, −12; MNI152: −45, −72, −10). These regions were created to serve as a reference for our own results and to perform statistical analyses.

Nevertheless, as there is an overlap between the aVWFA and cVWFA and the described regions left some empty spaces, we created the aa-ca-cp-pp set of regions as well (see c). This allowed us to systematically cover the litVWFA regions and, most importantly, the whole OTS along the anterior–posterior gradient, avoiding any overlaps and leaving no empty spaces. The subregions were created manually and called anterior–anterior (aa), central–anterior (ca), central–posterior (cp), and posterior–posterior (pp); hence, the set of the four regions was abbreviated to aa-ca-cp-pp.

To create the litVWFA set of regions, we converted the three MNI152 coordinates reported in the literature to the MNI305 space, selected the nearest surface vertex corresponding to the coordinate, and created one vertex 2D surface label. Then, using Freesurfer's mris_label_calc tool, each label was dilated eight times. The dilation factor was randomly chosen, yielding an approximate area (different for every subject) of 1.8 $cm^2$ (equivalent to a 1.3-cm side square).

***Functional statistical analyses.*** For every contrast and subject, the T value of the GMax inside the vOTC area and inside the abovementioned regions was located (with MNI X, Y, Z coordinates) and saved for analysis.

All analyses focused on the functional contrasts previously used in the scientific literature. First, we analyzed the most extensively used contrast, real word vs. fixation (RWvsNull), on its own. To statistically check the word selectivity gradient along the *y* axis, we performed a four (region) repeated-measures ANOVA to compare the T values inside each region.

Second, we examined the following six functional contrasts used in previous research: (*i*) RW vs. CB (RWvsCB), (*ii*) RW vs. SD (RWvsSD), (*iii*) RW vs. PS (RWvsPS), (*iv*) RW vs. PW (RWvsPW), (*v*) RW vs. CS (RWvsCS), and (*vi*) RW vs. FF (RWvsFF). First, we conducted a repeated-measures ANOVA using the GMax *y* value for each contrast as the dependent variable to test the hypothesis of a posterior–anterior gradient related to the PER/LEX nature of the contrasts. Then, we repeated the same analyses for the *x* and *z* axes to explore if there was an analogous functional gradient along these axes. To further examine to what extent the activations for the contrasts of interest organized as PER or LEX, we performed a hierarchical cluster analysis, as implemented by R's hclust (60), including each contrast's GMax T (mean and standard deviation) values.

Third, surface-based probabilistic maps were created for the aggregated PER and LEX functional contrasts. To this end, we first aggregated the six functional contrasts into PER and LEX contrasts. Then, we binarized the activations inside the OTS by using an individualized variable threshold (i.e., for every subject, all vertices that were at least 50% of their GMax were marked as one, and the rest were zeroed). Finally, with these binary values, we created a probabilistic map grouping all of the subject's values: A vertex would have a 100% value if all subjects had this vertex activated for a given contrast.

Fourth and last, ROI analyses were performed with the MARSBAR toolbox for use with SPM. Parameter estimates for the PER and LEX contrasts of interest were extracted per each subject from pOTS and mOTS 5-mm spheres ROIs (volume = 648 $mm^3$) centered at the local maxima to calculate percent signal change.

***Brain-behavior associations.*** To examine if functional activations within the vOTC for the functional contrasts of interest predicted individual reading ability, we conducted linear regression analyses at each vertex. The reading ability scores were obtained from the lexical decision task that participants performed outside the scanner. The complete analysis procedure consisted of the following steps: (*i*) RTs for CS and RW were obtained, removing RTs corresponding to incorrect trials, and values <200 ms and >2 standard deviations from the mean for correct trials; (*ii*) Functional activation maps were smoothed in the cortex using a Gaussian filter with a full-width at half-maximum of 5 mm; (*iii*) 12 different linear regressions were performed at each vertex inside the vOTC, using the functional activation T values (RWvsPS/CB/SD/PW/CS/FF) as independent variables and the behavioral data (CS and RW RTs) as dependent variables; and (*iv*) statistical cluster-wise corrections for multiple comparisons were carried out by using Freesurfer tools based on nonparametric Monte Carlo testing. We used an initial

cluster-forming vertex-wise threshold of $P < 0.05$, and only those clusters with a corrected value of $P < 0.05$ were considered statistically significant.

***Functional to structural correspondences.*** To examine the correspondence between the vOF and pAF cortical tract endings in the vOTC and our functional result coordinates in the pOTS and mOTS, we ran 2 $\chi^2$ tests, one per tract (vOF and pAF). To this end, we created a dichotomous variable per tract and region (pOTS and mOTS). For each subject, we indicated if the tract ending in question fell inside the region or not (at least one vertex). To examine the correspondence between the functional values and the T1 values, a simple *t* test with the average per-subject T1 values inside the pOTS and mOTS was performed.

***Test–retest validation for reproducibility of results.*** To check for the test–retest reliability of our results, we selected the acquisition sessions of the 31 subjects assigned to the test–retest experiment. These subjects had repeated the experiment after 7–10 d. For this experiment, the previously mentioned analyses were also conducted. For the ANOVAs an additional factor was included, test–retest: day 1, day 2. The rest of the tests were repeated with the retest group.

**ACKNOWLEDGMENTS.** We thank Brian A. Wandell for helpful discussions, Cesar Caballero-Gaudes and Silvia De Santis for technical support, and David Carcedo for help with data collection. This work was supported by European Molecular Biology Organization (EMBO, Short-Term Fellowship 158-2015) and Marie Sklodowska-Curie (H2020-MSCA-IF-2017-795807-ReCiModel) grants (to G.L.-U.); Spanish Ministry of Economy and Competitiveness (MINECO, PSI2015-67353-R, SEV-2015-0490) and European Research Council (ERC, ERC-2011-ADG-295362) grants (to M.C.); and MINECO (RYC-2014-15440, PSI2012-32093, SEV-2015-0490) and Departamento de Desarrollo Económico y Competitividad, Gobierno Vasco (PI2016-12) grants (to P.M.P.-A.).

1. Dehaene S, Cohen L, Sigman M, Vinckier F (2005) The neural code for written words: A proposal. *Trends Cogn Sci* 9:335–341.
2. Cohen L, et al. (2000) The visual word form area: Spatial and temporal characterization of an initial stage of reading in normal subjects and posterior split-brain patients. *Brain* 123:291–307.
3. Glezer LS, Riesenhuber M (2013) Individual variability in location impacts orthographic selectivity in the "visual word form area". *J Neurosci* 33:11221–11226.
4. Vogel AC, Petersen SE, Schlaggar BL (2012) The left occipitotemporal cortex does not show preferential activity for words. *Cereb Cortex* 22:2715–2732.
5. Saygin ZM, et al. (2016) Connectivity precedes function in the development of the visual word form area. *Nat Neurosci* 19:1250–1255.
6. Carreiras M, Armstrong BC, Perea M, Frost R (2014) The what, when, where, and how of visual word recognition. *Trends Cogn Sci* 18:90–98.
7. Vinckier F, et al. (2007) Hierarchical coding of letter strings in the ventral stream: Dissecting the inner organization of the visual word-form system. *Neuron* 55:143–156.
8. Bouhali F, et al. (2014) Anatomical connections of the visual word form area. *J Neurosci* 34:15402–15414.
9. Weiner KS, Yeatman JD, Wandell BA (2017) The posterior arcuate fasciculus and the vertical occipital fasciculus. *Cortex* 97:274–276.
10. Yeatman JD, et al. (2014) The vertical occipital fasciculus: A century of controversy resolved by in vivo measurements. *Proc Natl Acad Sci USA* 111:E5214–E5223.
11. Gomez J, et al. (2017) Microstructural proliferation in human cortex is coupled with the development of face processing. *Science* 355:68–71.
12. Rosenke M, et al. (2018) A cross-validated cytoarchitectonic atlas of the human ventral visual stream. *Neuroimage* 170:257–270.
13. Weiner KS, et al. (2017) The cytoarchitecture of domain-specific regions in human high-level visual cortex. *Cereb Cortex* 27:146–161.
14. Szwed M, et al. (2011) Specialization for written words over objects in the visual cortex. *Neuroimage* 56:330–344.
15. Price CJ, Noppeney U, Phillips J, Devlin JT (2003) How is the fusiform gyrus related to category-specificity? *Cogn Neuropsychol* 20:561–574.
16. Price CJ, Devlin JT (2011) The interactive account of ventral occipitotemporal contributions to reading. *Trends Cogn Sci* 15:246–253.
17. Kay KN, Yeatman JD (2017) Bottom-up and top-down computations in word- and face-selective cortex. *eLife* 6:e22341.
18. Caspers J, et al. (2013) Cytoarchitectonical analysis and probabilistic mapping of two extrastriate areas of the human posterior fusiform gyrus. *Brain Struct Funct* 218: 511–526.
19. Schenker-Ahmed NM, Annese J (2013) Cortical mapping by magnetic resonance imaging (MRI) and quantitative cytological analysis in the human brain: A feasibility study in the fusiform gyrus. *J Neurosci Methods* 218:9–16.
20. Dehaene S, Le Clec'H G, Poline JB, Le Bihan D, Cohen L (2002) The visual word form area: A prelexical representation of visual words in the fusiform gyrus. *Neuroreport* 13:321–325.
21. Cohen L, Jobert A, Le Bihan D, Dehaene S (2004) Distinct unimodal and multimodal regions for word processing in the left temporal cortex. *Neuroimage* 23:1256–1270.
22. Cohen L, et al. (2002) Language-specific tuning of visual cortex? Functional properties of the visual word form area. *Brain* 125:1054–1069.
23. Twomey T, Kawabata Duncan KJ, Price CJ, Devlin JT (2011) Top-down modulation of ventral occipito-temporal responses during visual word recognition. *Neuroimage* 55: 1242–1251.
24. Dehaene S, et al. (2010) How learning to read changes the cortical networks for vision and language. *Science* 330:1359–1364.
25. Yoncheva YN, Zevin JD, Maurer U, McCandliss BD (2010) Auditory selective attention to speech modulates activity in the visual word form area. *Cereb Cortex* 20:622–632.
26. Ben-Shachar M, Dougherty RF, Deutsch GK, Wandell BA (2007) Differential sensitivity to words and shapes in ventral occipito-temporal cortex. *Cereb Cortex* 17:1604–1611.
27. Ben-Shachar M, Dougherty RF, Wandell BA (2007) White matter pathways in reading. *Curr Opin Neurobiol* 17:258–270.
28. Dehaene S, Cohen L (2011) The unique role of the visual word form area in reading. *Trends Cogn Sci* 15:254–262.
29. Stevens WD, Kravitz DJ, Peng CS, Tessler MH, Martin A (2017) Privileged functional connectivity between the visual word form area and the language system. *J Neurosci* 37:5288–5297.
30. Yeatman JD, Rauschecker AM, Wandell BA (2013) Anatomy of the visual word form area: Adjacent cortical circuits and long-range white matter connections. *Brain Lang* 125:146–155.
31. Saygin ZM, et al. (2013) Tracking the roots of reading ability: White matter volume and integrity correlate with phonological awareness in prereading and early-reading kindergarten children. *J Neurosci* 33:13251–13258.
32. Thiebaut de Schotten M, Cohen L, Amemiya E, Braga LW, Dehaene S (2014) Learning to read improves the structure of the arcuate fasciculus. *Cereb Cortex* 24:989–995.
33. Oliver M, Carreiras M, Paz-Alonso PM (2017) Functional dynamics of dorsal and ventral reading networks in bilinguals. *Cereb Cortex* 27:5431–5443.
34. Hannagan T, Amedi A, Cohen L, Dehaene-Lambertz G, Dehaene S (2015) Origins of the specialization for letters and numbers in ventral occipitotemporal cortex. *Trends Cogn Sci* 19:374–382.
35. Dehaene S, Dehaene-Lambertz G (2016) Is the brain prewired for letters? *Nat Neurosci* 19:1192–1193.
36. Szwed M, Qiao E, Jobert A, Dehaene S, Cohen L (2014) Effects of literacy in early visual and occipitotemporal areas of Chinese and French readers. *J Cogn Neurosci* 26:459–475.
37. Pegado F, et al. (2014) Timing the impact of literacy on visual processing. *Proc Natl Acad Sci USA* 111:E5233–E5242.
38. Friston K (2010) The free-energy principle: A unified brain theory? *Nat Rev Neurosci* 11:127–138.
39. Tononi G, Sporns O, Edelman GM (1999) Measures of degeneracy and redundancy in biological networks. *Proc Natl Acad Sci USA* 96:3257–3262.
40. Brem S, et al. (2006) Evidence for developmental changes in the visual word processing network beyond adolescence. *Neuroimage* 29:822–837.
41. Brem S, et al. (2010) Brain sensitivity to print emerges when children learn letter-speech sound correspondences. *Proc Natl Acad Sci USA* 107:7939–7944.
42. van der Mark S, et al. (2011) The left occipitotemporal system in reading: Disruption of focal fMRI connectivity to left inferior frontal and inferior parietal language areas in children with dyslexia. *Neuroimage* 54:2426–2436.
43. Cohen L, Dehaene S (2004) Specialization within the ventral stream: The case for the visual word form area. *Neuroimage* 22:466–476.
44. Xue G, Poldrack RA (2007) The neural substrates of visual perceptual learning of words: Implications for the visual word form area hypothesis. *J Cogn Neurosci* 19: 1643–1655.
45. Stigliani A, Weiner KS, Grill-Spector K (2015) Temporal processing capacity in high-level visual cortex is domain specific. *J Neurosci* 35:12412–12424.
46. Jobard G, Crivello F, Tzourio-Mazoyer N (2003) Evaluation of the dual route theory of reading: A metanalysis of 35 neuroimaging studies. *Neuroimage* 20:693–712.
47. Kaufman AS (1990) Kaufman brief intelligence test: KBIT (American Guidance Service, Circle Pines, MN).
48. Kaplan E, Harold G, Weintraub S (1983) *Boston Naming Test* (Lea & Febiger, Philadelphia).
49. Duchon A, Perea M, Sebastián-Gallés N, Martí A, Carreiras M (2013) EsPal: One-stop shopping for Spanish word properties. *Behav Res Methods* 45:1246–1258.
50. Perea M, et al. (2006) E-Hitz: A word frequency list and a program for deriving psycholinguistic statistics in an agglutinative language (Basque). *Behav Res Methods* 38: 610–615.
51. Armstrong BC, Watson CE, Plaut DC (2012) SOS! an algorithm and software for the stochastic optimization of stimuli. *Behav Res Methods* 44:675–705.
52. Keuleers E, Brysbaert M (2010) Wuggy: A multilingual pseudoword generator. *Behav Res Methods* 42:627–633.
53. Mezer A, et al. (2013) Quantifying the local tissue volume and composition in individual brains with magnetic resonance imaging. *Nat Med* 19:1667–1672.
54. Fischl B, et al. (2004) Automatically parcellating the human cerebral cortex. *Cereb Cortex* 14:11–22.
55. Smith SM, et al. (2004) Advances in functional and structural MR image analysis and implementation as FSL. *Neuroimage* 23(Suppl 1):S208–S219.
56. Jeurissen B, Tournier JD, Dhollander T, Connelly A, Sijbers J (2014) Multi-tissue constrained spherical deconvolution for improved analysis of multi-shell diffusion MRI data. *Neuroimage* 103:411–426.
57. Tournier J-D, Calamante F, Connelly A (2010) Improved probabilistic streamlines tractography by 2nd order integration over fibre orientation distributions. *Proceedings of 18th Annual Meeting of the International Society for Magnetic Resonance in Medicine* (International Society for Magnetic Resonance in Medicine, Concord, CA), p 1670.
58. Yeatman JD, Dougherty RF, Myall NJ, Wandell BA, Feldman HM (2012) Tract profiles of white matter properties: Automating fiber-tract quantification. *PLoS One* 7:e49790.
59. Mazaika PK, Hoeft F, Glover GH, Reiss AL (2009) Methods and software for fMRI analysis of clinical subjects. *Neuroimage* 47(Suppl 1):S58.
60. Murtagh F (1985) Multidimensional clustering algorithms. *Compstat Lectures* (Physika, Vienna).